3D Orientation of Single Gold Bipyramid Measured by Scattering Polarization pectroscopy: Role of the Numerical Aperture

Cam Vu, Zakarya Ouzit, Clotilde Lethiec, Agnès Maitre, Laurent Coolen, Frédéric Lerouge, Michel Pellarin, Julien Laverdant

Sensors & Transducers, Vol. 255, Issue 1, January 2022, pp. 10-16

www.sensorsportal.com

Sensors & Transducers

Published by IFSA Publishing, S. L., 2022
http://www.sensorsportal.com

3D Orientation of Single Gold Bipyramid Measured by Scattering Polarization Spectroscopy: Role of the Numerical Aperture

[1, *] Cam Nhung VU, [2] Zakarya OUZIT, [2] Clotilde LETHIEC, [2] Agnès MAITRE, [2] Laurent COOLEN, [3] Frédéric LEROUGE, [1] Michel PELLARIN [1] and Julien LAVERDANT

[1] Institut Lumière Matière, Université Claude Bernard Lyon 1, CNRS, Université de Lyon, F-69622 Villeurbanne, France

[2] Sorbonne Université, CNRS, Institut de NanoSciences de Paris, INSP, F-75005 Paris, France

[3] Univ Lyon, Ens de Lyon, CNRS, Université Lyon 1, Laboratoire de Chimie UMR 5182, F-69342, Lyon, France

[*] E-mail: nhungvu.phys@gmail.com

Received: 3 December 2021 /Accepted: 11 January 2022 /Published: 31 January 2022

Abstract: The 3D orientation of a single gold nano-bipyramid (AuBPs) on a glass substrate is successfully measured by polarimetric analysis of its scattering. The AuBPs are very attractive due to the presence of hot spots at their end tips resulting from a strong longitudinal localized surface plasmon resonance. In addition, this resonance can be modeled as a radiating dipole. To study the 3D orientation, we designed a specific spectroscopic dark-field microscope with a precise control of the collection angles of the scattering in the Fourier plane. The 3D angles are resolved by analyzing the polarization of the AuBP scattering. Simulations are used to extract the in-plane and out-of-plane angles with a very good accuracy of 3 %. In particular, the critical role of the numerical aperture collection was investigated experimentally by Fourier filtering of the scattering into the back focal plane of the objective. It reveals a physical insight into the contribution of the evanescence waves and provides a technical guideline for choosing the collection objective for polarimetric measurements.

Keywords: Localized surface plasmon, Gold bipyramids, Orientation, Polarization, Scattering.

1. Introduction

The determination of the orientation of nanoparticles at the single level is a key point for many applications in sensing [1, 2], coupling [3-5], and all interaction effects [6-10]. It comes from the fact that the optical response of a nano-object is sufficiently sensitive to its local environments, e.g. refractive index, that depends on the orientation of the particles. This dependence is especially significant in the situation of an elongated nanoparticle is in the vicinity of a substrate [38] where the inclination of the particles leads to several differences in scattering resonances since it decides how much the particle is exposed to the substrate index. Furthermore, the orientation is also a crucial parameter to optimize the coupling strength of an emitter inside plasmonic nanocavities. On these, a strong coupling may be achieved for emitters that are grafted following the direction of the local field inside the cavities [10, 11].

For these applications, the dye molecules, semiconductor nanocrystals, and plasmonic nanostructures have been widely used thanks to their excellent optical responses. Otherwise, plasmonic nanoparticles have a large scattering and absorption cross-section, and do not suffer from major drawbacks of the fluorescence emitters such as photoblinking [12, 13] or instability from biochemical environment [14, 15]. This comes from the ability to confine the field at the nanoscale of the noble metallic nanoparticles that emerges from a phenomenon which is known as localized surface plasmon resonance (LSPR) [16-19]. The LSPR effect becomes especially important for anisotropic plasmonic nanoparticles where gold bipyramids (AuBPs) stand as a promising candidate in recent years due to several desirable properties. The AuBPs have a high aspect ratio as common elongated plasmonic nanoparticles while own sharp curvature at the tip ends showing better local field confinement and enhancement [2]. Therefore, our work in this paper aims to determine 3D orientation of the AuBPs at the single particle level.

Various optical methods have been early developed such as radiation pattern or polarization analysis. Among the patterning methods, we can cite the defocused imaging [20, 21], and Fourier plane imaging [22-25] which offers the most convenient implementation. The orientation of the particles can be deduced from the projection of the radiation pattern on these planes. However, the angular resolved imaging usually demands highly sensitive detectors. In particular, the defocused imaging is also very sensitive to the alignment and aberrations of the experiment setup. Despite all of the strict requirements, these methods cannot be applied to all circumstances. For example, the orientation of quantum dots on an absorbing substrate is not resolved by the Fourier plane imaging [26]. On the other hand, the polarimetric analysis methods have shown good precision without rigorous requirements as the radiation pattern imaging methods [27-35]. One way is to split the optical response of nanoparticles into two orthogonal polarization directions to measure the optical anisotropy [30, 32]. However, the anisotropy measurement is only effective for the determination of the in-plane orientation.

In the presented work, we present a method to retrieve the 3D orientation of single nanoparticles based on resolved polarimetric scattering spectrum. The work goes further on investigating the role of the numerical aperture of the collection since the polarization states are not similar in different radiation directions. The developed method is then applied on gold bipyramid nanoparticles (AuBPs) that is an interesting model system for single-emitter light scattering. The AuBPs mainly support a strong longitudinal localized surface plasmon resonance owing to its very sharp end tips (other modes with very low scattering cross-sections can be neglected). This longitudinal resonance is easily tuned by playing with the aspect ratio of the particle [22, 23]. In terms of theoretical calculation, the longitudinal mode of the AuBPs can be modeled as a linear radiating dipole. In addition, the AuBPs allow access to out-of-plane angles without any surface treatment thanks to the geometry of the bipyramid.

2. 3D Orientation Measurement of a Single Gold Bipyramid

2.1. Theoretical Calculation of Polarization Analysis

Theoretical calculation is described in our previous work [26]. In this, the nanoparticle is modeled as a dipole radiating through an air-glass interface that is then collected by an objective. A polarizer with rotating angle α is placed on the detection pathway. The detected intensity oscillates between a maximum (I_{max}) and a minimum (I_{min}) values with the variation of the angle α, following the Malus's law:

$$\mathrm{I}(\alpha) = I_{min} + (I_{max} - I_{min})cos^2(\phi - \alpha) \qquad (1)$$

For the linear dipole (1D), the I_{max} is retrieved when the polarizer in the parallel direction to the dipole axis while for the orthogonal direction, the intensity is minimum. From the Eq. (1), the in – plane angle ϕ is directly retrieved.

It is important to note that the calculation has taken into account parameters of the local environment as well as the numerical aperture of the objective. At a fixed numerical aperture (NA) of a collection objective, the out – of – plane angle Θ is determined using the measured degree of polarization (DOP) δ, obtained as:

$$\delta_{\mathrm{NA}} = \frac{I_{max} - I_{min}}{I_{max} + I_{min}} \qquad (2)$$

2.2. Numerical Investigation of Scattering of Single Gold Bipyramid

The scattering spectrum of the AuBPs are investigated numerically by finite element methods (COMSOL, 5.2 software). The sizes of the AuBPs are 100 nm long and 30 nm in width (square base). The tips are slightly truncated with a square basis of 3 nm width. The geometry size of the AuBPs is deduced from the size distribution measured by scanning electron microscope (SEM). In the simulation, the AuBP is placed glass substrate with an angle of 15° and excited by a plane wave in normal incidence (Fig. 1). Under a plane wave excitation, the charges are mainly distributed at the two end tips of the AuBP results in a strong scattering resonance at 740 nm. Thus, this mode behaves like a linear radiating dipole. The two very weak modes at lower wavelength are respectively quadrupolar mode and transverse mode of the charge oscillation that are neglected in our measurement.

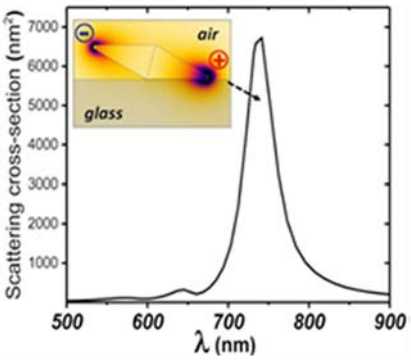

Fig. 1. Numerical simulations of the AuBP optical properties. Scattering spectrum together with, in insert, the charge distribution associated at the main resonance (740 nm).

The longitudinal surface plasmon mode of the AuBPs has dipolar nature that is spatially modified by the local environment [35], particularly in this case is the glass substrate. Therefore, we make a calculation of the scattering diagram of an AuBP in a vicinity of the glass substrate. In the calculation, the particle is modelled as a linear dipole. The far-field radiation of the dipole is collected in the semi-infinite medium of the glass (n = 1.5) by an oil matching index objective. Herein, the objective is approximately simulated as a reference sphere that converts the light into a collimated beam with a planar wave front. The emission diagram is presented as the angular distribution of the intensities radiating from the dipole $I(\theta, \varphi)$ on the Fourier plane of the objective. Due to the planar symmetry, the radiated electric field is presented in terms of p and s polarizations. The angular distribution of the radiating intensity $I(\theta, \varphi)$is express as [24]:

$$I(\theta, \varphi, \Theta, \Phi) \sim \frac{1}{cos\theta} . \left(E_s . E_s^* + E_p . E_p^*\right) \qquad (3)$$

In which, (1/cos θ) is the apodization factor which is the result of the sine condition and the energy conservation when a focused beam passing through an objective. The electric field components p and s are also functions of dipole orientation (Θ, Φ) and observation angles (θ, ϕ) (Fig. 2a), their expressions are given as:

$$\begin{aligned} E_s(\theta, \varphi) &= a_1(\theta, \varphi) . sin\Theta . sin(\varphi - \Phi), \\ E_p(\theta, \varphi) &= E_p^{par}(\theta, \varphi) + E_p^{ver}(\theta, \varphi) \end{aligned} \qquad (4)$$

with

$$\begin{aligned} E_p^{par}(\theta, \varphi) &= a_2(\theta, \varphi) . sin\Theta . cos(\varphi - \Phi), \\ E_p^{par}(\theta, \varphi) &= a_3(\theta, \varphi) . cos\Theta . \sin\theta \end{aligned}$$

In which, the functions $a_1(\theta, \varphi)$, $a_2(\theta, \varphi)$, and $a_3(\theta, \varphi)$ related to the transmission coefficient of the air/glass interface. The expressions of these functions can be found in the reference [24].

The spatial distribution of intensity $I(\theta, \varphi)$on the Fourier plane of the objective is represented in terms of the wavevectors, denoted as $k_x = n . sin\theta . cos\varphi$ and $k_y = n . sin\theta . sin\varphi$. Fig. 2b shows an emission diagram on the Fourier plane $I(k_x, k_y)$ of a dipole inclined an angle of Θ = 15° to the glass substrate. As the numerical aperture of the objective $NA = n . sin\theta$, the radius of the emission diagram is limited by this parameter. In this case, the modelled objective has NA = 1.49. It is worth noting that since the dipole radiating through the air/glass interface, the solid angle corresponding to NA = 1 is the critical angle defined by refractive indices of these media. The emission diagram shows that the radiation is strongly modified by the presence of the interface toward the higher index medium (glass). Especially, the interface redistributed the radiation mainly into the evanescent regime corresponding to NA = [1, 1.49]. Besides, the influence of the out-of-plane orientation Θ = 15° is observed as the contrast of the intensities along the dipole axis.

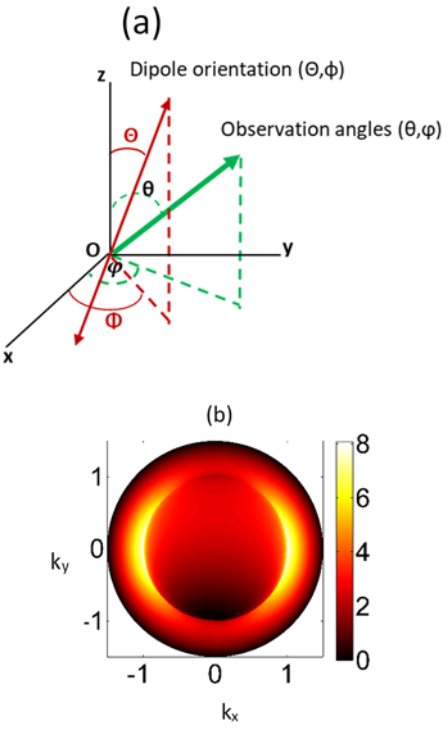

Fig. 2. (a) Schematic of the spherical coordinates defining the orientation of the dipole (Θ, Φ) and the direction of the observation (θ, ϕ); (b) Simulated emission diagram on the Fourier plane of the objective of a dipole inclined 15° to the substrate.

2.3. Experiment Set Up

Fig. 3 illustrates the experimental set up which combines dark-field imaging and Fourier filtering.

The AuBPs are deposited on a glass substrate and excited by a white lamp focused by a low numerical aperture (NA) objective and then both direct

illumination and scattered light are collected by an oil objective with NA = 1.49. A beam blocker is placed at the Fourier-plane position (F'.P') to effectively block the overwhelming illumination and retain only the scattering. At the same time, a diaphragm is also set at this position to control the scattering collection NA. It is worth mentioning that the primary Fourier plane of the oil objective is usually inside or very near the objective pupil. Therefore, a conjugated lens system is used to displace the Fourier plane to a convenient position for collection manipulation. The polarization analysis of the scattered light is then conducted by combining a rotating half-wave plate (λ/2) and a fixed polarizer (P).

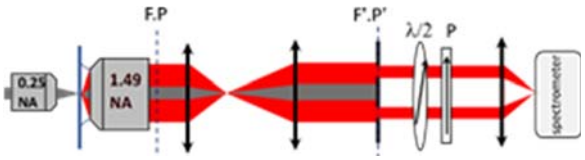

Fig. 3. Schematic of the experimental set up. F.P: the primary Fourier plane, F'.P': the image of the Fourier plane, λ/2: the rotating half-wave plate, and P: the fixed polarizer.

3. Results and Discussion

3.1. Dark-field Imaging

Fig. 4a shows a dark-field image of the AuBPs deposited on the glass substrate that was measured by the experiment setup in Fig. 3.

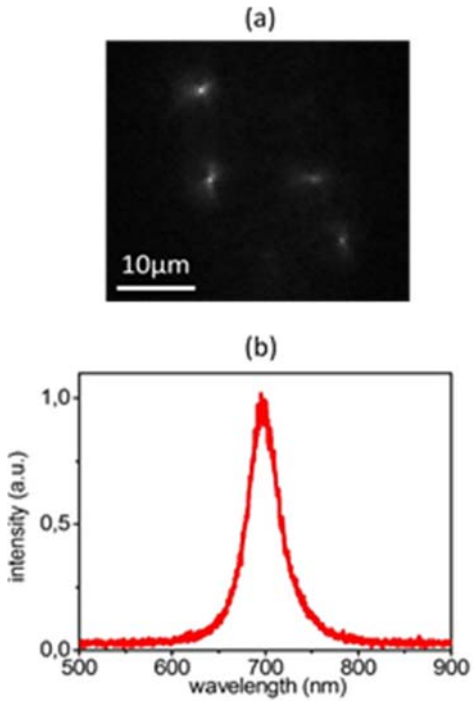

Fig. 4. (a) Dark-field image of the AuBPs deposited on the glass substrate; (b) Scattering spectrum of a single selected AuBP.

The bright spots come from the scattering of the nanoparticles while the dark background proves that the overwhelming illumination was sufficiently filtered out. Especially, the AuBPs are very well separated from each other allowing to measure scattering at the single level.

A scattering spectrum of a selected AuBP is presented in Fig. 4b where the resonance wavelength is located around 700 nm associated with the longitudinal mode. Besides, the width of the spectrum is narrow, around 50 nm, which is usually an optical response achieved from a single nano-object at the ambition condition.

3.2. 3D Orientation of the AuBPs

The polarimetric measurements are performed on the high quality AuBPs with average length of 100 nm and aspect ratio around 3.3 supporting a well – defined longitudinal resonance between 650 - 750 nm. The synthesis protocol can be found in [2]. Fig. 5 plots the obtained results of orientation measurement.

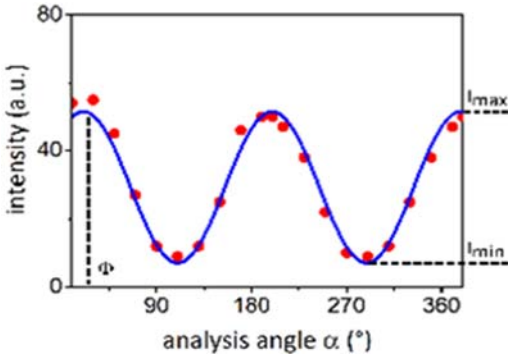

Fig. 5. Detected intensity (red dots) as a function of analysis angle α fit with the Eq. (1) (blue curve).

The evolution of the intensity as a function of the analysis angle α follows very well the Eq. (1). From the fit, three parameters are extracted: the in-plane angle Φ, the maximum, and the minimum intensities (I_{max} and I_{min}). In which, the in-plane angle is defined as analysis angle at the first maximum value of the detected intensity. We find for this AuBP, an in-plane angle Φ = 30° and a DOP δ = 0.72 with 3 % of precision. From the Eq. (2), we deduce out-of-plane angle Θ = 75°.

The degree of polarization and deduced out-of-plane angle measurement are then repeated for 30 other AuBPs (Fig. 6). We found that the AuBPs possess distributed out-of-plane angles between 60° and 90°, in which the 70-80° orientations are dominant. This distribution is consistent with the shape and the size of the AuBPs deduced from the electronic microscope measurement. There are considerable numbers of AuBPs paralleled with the substrate that might be induced from ligands surrounding the particle.

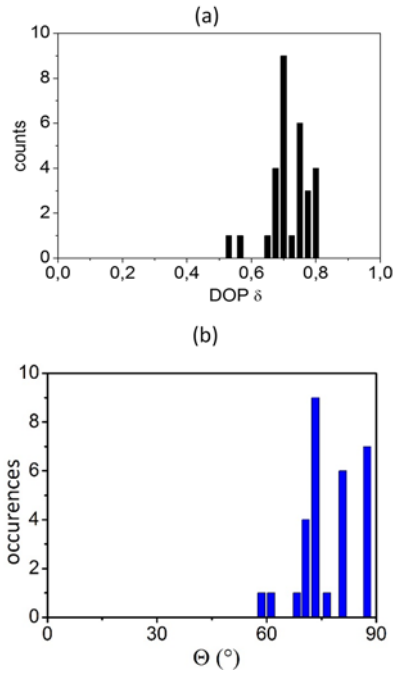

Fig. 6. Histogram of (a) degree of polarization and (b) out-of-plane orientation of 30 AuBPs measured by polarization analysis.

3.3. Role of Collection Numerical Aperture

The simulation indicates that the strong longitudinal surface plasmon resonance mode of the AuBPs behaves like a linear radiating dipole. When they are near an air/glass interface, the scattering is mainly radiated in the forbidden region above the critical angle [39]. Fig. 7 simulates the 3D radiation pattern of a dipole placed in air and near a glass substrate that is strongly redistributed toward the higher index medium.

The Fourier plane is the projection of the radiation pattern where each point on the Fourier plane corresponds to one direction of the radiation. Herein, the polarization states of different radiation directions have been presented (blue arrows). It is clear that the polarization states are not homogeneous on the entire Fourier plane. They become more complicated with the increase of numerical aperture, especially near the critical region around NA = 1. In other words, the polarization states are also strongly redistributed. Thus, in terms of the experiment, the collected NA of the objective plays an important role on the orientation measurements. In order to illustrate this dependence, we performed the polarization measurements with angular filtering. The results are displayed in Fig. 8.

Fig. 8 presents the DOP as a function of NA which is artificial changed from 0.45 – 1.49 by Fourier filtering (Fig. 3). We see that at low NA, δ nearly reaches unity but when the diaphragm is larger, it drops by 30 %, and more significantly around NA = 1. When the NA increases, the scattering is collected into different directions which possess specific polarization angles result in the decrease of the DOP. It is worth noting that the detected intensities also strongly depend on the NA collection, therefore, the choice of an optimal objective is a compromise between a fast variation of the δ(Θ) and an effective collection efficiency.

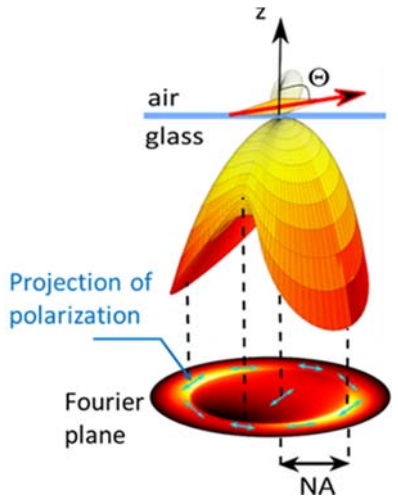

Fig. 7. Simulation of the 3D radiation pattern and the Fourier plane image of a dipole near air/glass interface. The projection of polarizations on the Fourier plane is showed as blue arrows.

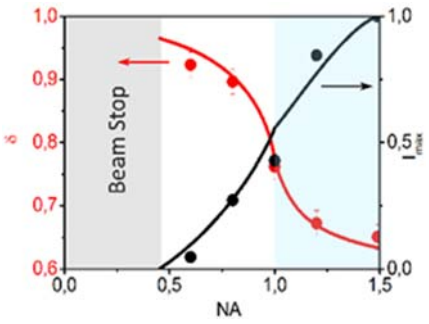

Fig. 8. DOP (red) and I_{max} (black) as functions of collection NA. Dots: experimental values. Curves: simulation.

3.4. Microscope Objective for the Polarimetric Measurement

As the DOP is strongly influenced by the collected NA, the choice of the objective for the polarimetric measurements is crucial. Fig. 9 shows the evolution of the degree of polarization (DOP) δ as the function of the out – of – plane orientation Θ with different collection: NA = 1.15 and NA = 1.49 represent for oil objectives, while NA = 0.5 and NA = 0.9 stand for air objectives.

The theoretical calculation on Fig. 9a has taken into account the experimental parameters with the presence of the beam stop 0.45NA. There is a minor difference compared to the case of collection in a full solid angle (Fig. 9b) because some polarization directions below the solid angle NAc =0.45 are cut – off by the beam stop. In the grey zones, the δ is nearly constant with collection in the large NA while its

variation is bigger in the case of collection in the small NA. In the opposite, when the dipole is nearly in the plane of the substrate (Θ = 70 – 90°), it is difficult to measure variations of δ for objectives with small NA.

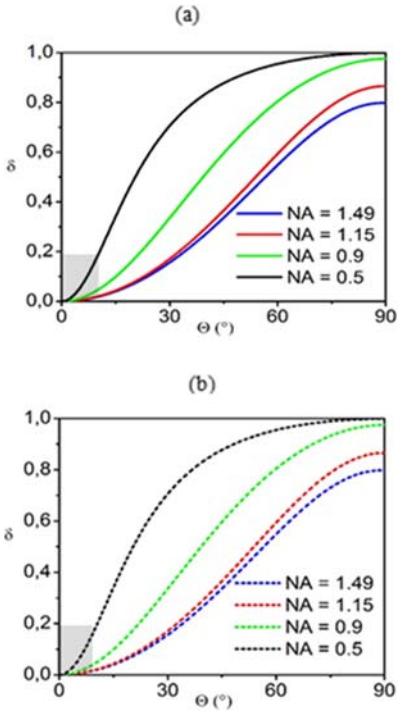

Fig. 9. Theoretical calculations of the DOP as a function of the dipole orientation Θ for two configurations of collection: (a) with the beam stop limiting NA = 0.45, and (b) for a full collection. Four different objective numerical apertures are evaluated for each configuration. The grey zones correspond to dipoles which are oriented nearly vertical (Θ = 0 – 10°).

4. Conclusions

In conclusion, we showed that the complete orientation of the AuBPs has been successfully resolved by the scattering polarimetry spectroscopy. Most of the particles exhibited the out-of-plane orientation on the substrate which is consistent with their geometry. The crucial role of the collection numerical aperture has been addressed, both experimentally and theoretically. We also show that depending on the orientation, the choice of the microscope objective NA is crucial. Our original method to obtain the direct dependence of the polarization on the objective NA may be applied for more complex systems with different radiation pattern.

Acknowledgements

We acknowledge the French Région Auvergne-Rhône-Alpes (SCUSI no 1700936601) that supported this work and the USTH French consortium.

References

[1]. T. Shegai, P. Johansson, C. Langhammer, M. Käll, Directional Scattering and Hydrogen Sensing by Bimetallic Pd–Au Nanoantennas, *Nano Letters*, Vol. 12, Issue 5, 2012, pp. 2464-2469.

[2]. J. Rye, C. Bonnet, F. Lerouge, M. Pellarin, J. Lermé, S. Parola, E. Cottancin, Single gold bipyramids on a silanized substrate as robust plasmonic sensors for liquid environments, *Nanoscale*, Vol. 10, Issue 34, 2018, pp. 16094-16101.

[3]. C. Tabor, D. Van Haute, M. El-Sayed, Effect of Orientation on Plasmonic Coupling between Gold Nanorods, *ACS Nano*, Vol. 3, Issue 11, 2009, pp. 3670-3678.

[4]. S. Kühn, U. Håkanson, L. Rogobete, V. Sandoghdar, Enhancement of Single-Molecule Fluorescence Using a Gold Nanoparticle as an Optical Nanoantenna, *Physical Review Letters*, Vol. 97, Issue 1, 2006.

[5]. P. Anger, P. Bharadwaj, L. Novotny, Enhancement and Quenching of Single-Molecule Fluorescence, *Physical Review Letters*, Vol. 96, Issue 11, 2006.

[6]. R. Chikkaraddy, B. de Nijs, F. Benz, S. Barrow, O. Scherman, E. Rosta, A. Demetriadou, P. Fox, O. Hess, J. Baumberg, Single-molecule strong coupling at room temperature in plasmonic nanocavities, *Nature*, Vol. 535, Issue 7610, 2016, pp. 127-130.

[7]. G. Akselrod, C. Argyropoulos, T. Hoang, C. Ciracì, C. Fang, J. Huang, D. Smith, M. Mikkelsen, Probing the mechanisms of large Purcell enhancement in plasmonic nanoantennas, *Nature Photonics*, Vol. 8, Issue 11, 2014, pp. 835-840.

[8]. J. Baumberg, J. Aizpurua, M. Mikkelsen, D. Smith, Extreme nanophotonics from ultrathin metallic gaps, *Nature Materials*, Vol. 18, Issue 7, 2019, pp. 668-678.

[9]. T. Hoang, G. Akselrod, C. Argyropoulos, J. Huang, D. Smith, M. Mikkelsen, Ultrafast spontaneous emission source using plasmonic nanoantennas, *Nature Communications*, Vol. 6, Issue 1, 2015.

[10]. T. Hoang, G. Akselrod, M. Mikkelsen, Ultrafast Room-Temperature Single Photon Emission from Quantum Dots Coupled to Plasmonic Nanocavities, *Nano Letters*, Vol. 16, Issue 1, 2015, pp. 270-275.

[11]. A. Dhawan, C. Belacel, J. Esparza-Villa, M. Nasilowski, Z. Wang, C. Schwob, J. Hugonin, L. Coolen, B. Dubertret, P. Senellart, A. Maître, Extreme multiexciton emission from deterministically assembled single-emitter subwavelength plasmonic patch antennas, *Light: Science & Applications*, Vol. 9, Issue 1, 2020.

[12]. F. Hu, Z. Cao, C. Zhang, X. Wang, M. Xiao, Defect-Induced Photoluminescence Blinking of Single Epitaxial InGaAs Quantum Dots, *Scientific Reports*, Vol. 5, Issue 1, 2015.

[13]. E. Riley, C. Hess, P. Reid, Photoluminescence Intermittency from Single Quantum Dots to Organic Molecules: Emerging Themes, *International Journal of Molecular Sciences*, Vol. 13, Issue 12, 2012, pp. 12487-12518.

[14]. C. Eggeling, J. Widengren, R. Rigler, C. Seidel, Photobleaching of Fluorescent Dyes under Conditions Used for Single-Molecule Detection: Evidence of Two-Step Photolysis, *Analytical Chemistry*, Vol. 70, Issue 13, 1998, pp. 2651-2659.

[15]. C. Eggeling, J. Widengren, R. Rigler, C. Seidel, Photobleaching of Fluorescent Dyes under Conditions Used for Single-Molecule Detection: Evidence of

Two-Step Photolysis, *Analytical Chemistry*, Vol. 70, Issue 13, 1998, pp. 2651-2659.
[16]. K. Mayer, J. Hafner, Localized Surface Plasmon Resonance Sensors, *Chemical Reviews*, Vol. 111, Issue 6, 2011, pp. 3828-3857.
[17]. H. Jeon, P. Tsalu, J. Ha, Shape Effect on the Refractive Index Sensitivity at Localized Surface Plasmon Resonance Inflection Points of Single Gold Nanocubes with Vertices, *Scientific Reports*, Vol. 9, Issue 1, 2019.
[18]. P. Zijlstra, P. Paulo, M. Orrit, Optical detection of single non-absorbing molecules using the surface plasmon resonance of a gold nanorod, *Nature Nanotechnology*, Vol. 7, Issue 6, 2012, pp. 379-382.
[19]. W. Shang, F. Xiao, W. Zhu, L. Han, T. Mei, J. Zhao, Characterizing localized surface plasmon resonances using focused radially polarized beam, *Applied Optics*, Vol. 58, Issue 21, 2019, pp. 5812-5816.
[20]. L. Xiao, Y. Qiao, Y. He, E. Yeung, Three Dimensional Orientational Imaging of Nanoparticles with Darkfield Microscopy, *Analytical Chemistry*, Vol. 82, Issue 12, 2010, pp. 5268-5274.
[21]. S. Lee, Y. Han, J. Hong, J. Ha, Single gold bipyramids with sharp tips as sensitive single particle orientation sensors in biological studies, *Nanoscale*, Vol. 9, Issue 33, 2017, pp. 12060-12067.
[22]. T. Zhang, H. Shen, G. Lu, J. Liu, Y. He, Y. Wang, Q. Gong, Single Bipyramid Plasmonic Antenna Orientation Determined by Direct Photoluminescence Pattern Imaging, *Advanced Optical Materials*, Vol. 1, Issue 4, 2013, pp. 335-342.
[23]. C. Huang, A. Bouhelier, G. Colas des Francs, A. Bruyant, A. Guenot, E. Finot, J. Weeber, A. Dereux, Gain, detuning, radiation patterns of nanoparticle optical antennas, *Physical Review B*, Vol. 78, Issue 15, 2008.
[24]. R. Chacon, A. Leray, J. Kim, K. Lahlil, S. Mathew, A. Bouhelier, J. Kim, T. Gacoin, G. Colas des Francs, Measuring the Magnetic Dipole Transition of Single Nanorods by Spectroscopy, Fourier Microscopy, *Physical Review Applied*, Vol. 14, Issue 5, 2020.
[25]. J. Liu, A. Maître, L. Coolen, Tailoring Experimental Configurations to Probe Transition Dipoles of Fluorescent Nanoemitters by Polarimetry or Fourier Imaging with Enhanced Sensitivity, *The Journal of Physical Chemistry A*, Vol. 125, Issue 34, 2021, pp. 7572-7580.
[26]. C. Lethiec, J. Laverdant, H. Vallon, C. Javaux, B. Dubertret, J. Frigerio, C. Schwob, L. Coolen, A. Maître, Measurement of Three-Dimensional Dipole Orientation of a Single Fluorescent Nanoemitter by Emission Polarization Analysis, *Physical Review X*, Vol. 4, Issue 2, 2014.
[27]. C. Lethiec, F. Pisanello, L. Carbone, A. Bramati, L. Coolen, A. Maître, Polarimetry-based analysis of dipolar transitions of single colloidal CdSe/CdS dot-in-rods, *New Journal of Physics*, Vol. 16, Issue 9, 2014, p. 093014.
[28]. T. Ha, T. Laurence, D. Chemla, S. Weiss, Polarization Spectroscopy of Single Fluorescent Molecules, *The Journal of Physical Chemistry B*, Vol. 103, Issue 33, 1999, pp. 6839-6850.
[29]. W. Chang, J. Ha, L. Slaughter, S. Link, Plasmonic nanorod absorbers as orientation sensors, *Proceedings of the National Academy of Sciences*, Vol. 107, Issue 7, 2010, pp. 2781-2786.
[30]. J. Lee, Z. Cheglakov, J. Yi, T. Cronin, K. Gibson, B. Tian, Y. Weizmann, Plasmonic Photothermal Gold Bipyramid Nanoreactors for Ultrafast Real-Time Bioassays, *Journal of the American Chemical Society*, Vol. 139, Issue 24, 2017, pp. 8054-8057.
[31]. F. Feng, L. Nguyen, M. Nasilowski, B. Nadal, B. Dubertret, A. Maître, L. Coolen, Probing the Fluorescence Dipoles of Single Cubic CdSe/CdS Nanoplatelets with Vertical or Horizontal Orientations, *ACS Photonics*, Vol. 5, Issue 5, 2018, pp. 1994-1999.
[32]. I. Chung, K. Shimizu, M. Bawendi, Room temperature measurements of the 3D orientation of single CdSe quantum dots using polarization microscopy, *Proceedings of the National Academy of Sciences of the United States of America*, Vol. 100, Issue 2, 2003, pp. 405-408.
[33]. J. Kim, R. Chacón, Z. Wang, E. Larquet, K. Lahlil, A. Leray, G. Colas-des-Francs, J. Kim, T. Gacoin, Measuring 3D orientation of nanocrystals via polarized luminescence of rare-earth dopants, *Nature Communications*, Vol. 12, Issue 1, 2021.
[34]. J. Liu, A. Maître, L. Coolen, Tailoring Experimental Configurations to Probe Transition Dipoles of Fluorescent Nanoemitters by Polarimetry or Fourier Imaging with Enhanced Sensitivity, *The Journal of Physical Chemistry A*, Vol. 125, Issue 34, 2021, pp. 7572-7580.
[35]. N. C. Vu, Z. Ouzit, A. Maitre, L. Coolen, F. Lerouge, J. Laverdant, Single Gold Bipyramid Orientation measured by Plasmon-Resonant Scattering Spectroscopy, in *Proceeding of 4th International Conference on Optics, Photonics, lasers (OPAL'2021)*, Corfu, Greece, 13-15 October 2021, pp. 36-38.
[36]. J. Navarro, D. Manchon, F. Lerouge, N. Blanchard, S. Marotte, Y. Leverrier, J. Marvel, F. Chaput, G. Micouin, A. Gabudean, A. Mosset, E. Cottancin, P. Baldeck, K. Kamada, S. Parola, Synthesis of PEGylated gold nanostars, bipyramids for intracellular uptake, *Nanotechnology*, Vol. 23, Issue 46, 2012, p. 465602.
[37]. J. Navarro, D. Manchon, F. Lerouge, E. Cottancin, J. Lermé, C. Bonnet, F. Chaput, A. Mosset, M. Pellarin, S. Parola, Synthesis, electron tomography, single-particle optical response of twisted gold nano-bipyramids, *Nanotechnology*, Vol. 23, Issue 14, 2012, p. 145707.
[38]. A. Lombardi, M. Loumaigne, A. Crut, P. Maioli, N. Del Fatti, F. Vallée, M. Spuch-Calvar, J. Burgin, J. Majimel, M. Tréguer-Delapierre, Surface Plasmon Resonance Properties of Single Elongated Nano-objects: Gold Nanobipyramids, Nanorods, *Langmuir*, Vol. 28, Issue 24, 2012, pp. 9027-9033.
[39]. Novotny L., Hecht B., Principle of Nano-Optics, *Cambridge University Press,* Cambridge, U.K., 2006.